THE JOURNAL OF BIOLOGICAL CHEMISTRY VOL. 288, NO. 2, pp. 1150–1161, January 11, 2013


# Molecular Interaction Studies of HIV-1 Matrix Protein p17 and Heparin

## *IDENTIFICATION OF THE HEPARIN-BINDING MOTIF OF p17 AS A TARGET FOR THE DEVELOPMENT OF MULTITARGET ANTAGONISTS**

Received for publication, July 12, 2012, and in revised form, November 5, 2012 Published, JBC Papers in Press, November 19, 2012, DOI 10.1074/jbc.M112.400077

**Antonella Bugatti[‡], Cinzia Giagulli[§], Chiara Urbinati[‡], Francesca Caccuri[§], Paola Chiodelli[‡], Pasqua Oreste[¶], Simona Fiorentini[§], Alessandro Orro[‖], Luciano Milanesi[‖], Pasqualina D'Ursi[‖], Arnaldo Caruso[§], and Marco Rusnati[‡1]**

*From the [‡]Section of Experimental Oncology and Immunology and [§]Section of Microbiology, Department of Molecular and Translational Medicine, School of Medicine, University of Brescia, Brescia 25123, Italy, [¶]Glycores 2000A 20155, Milan, Italy, and the [‖]Institute for Biomedical Technologies-National Research Council, Segrate 20090, Italy*

**Background:** HIV-1 p17 binds heparin and heparan sulfate proteoglycans of the cell surface.
**Results:** Heparin/p17 interaction occurs through heparin sulfate groups and a linear basic motif of p17 N terminus, also involved in p17/CXCR1 interaction.
**Conclusion:** Targeting the basic motif inhibits p17-receptors interaction and consequent biological activities.
**Significance:** Heparin-like molecules represent template for the development of new treatments of p17-dependent/AIDS-associated pathologies.

**Once released by HIV$^+$ cells, p17 binds heparan sulfate proteoglycans (HSPGs) and CXCR1 on leukocytes causing their dysfunction. By exploiting an approach integrating computational modeling, site-directed mutagenesis of p17, chemical desulfation of heparin, and surface plasmon resonance, we characterized the interaction of p17 with heparin, a HSPG structural analog, and CXCR1. p17 binds to heparin with an affinity ($K_d$ = 190 nM) that is similar to those of other heparin-binding viral proteins. Two stretches of basic amino acids (basic motifs) are present in p17 N and C termini. Neutralization (Arg→Ala substitution) of the N-terminal, but not of the C-terminal basic motif, causes the loss of p17 heparin-binding capacity. The N-terminal heparin-binding motif of p17 partially overlaps the CXCR1-binding domain. Accordingly, its neutralization prevents also p17 binding to the chemochine receptor. Competition experiments demonstrated that free heparin and heparan sulfate (HS), but not selectively 2-*O*-, 6-*O*-, and *N*-*O* desulfated heparins, prevent p17 binding to substrate-immobilized heparin, indicating that the sulfate groups of the glycosaminoglycan mediate p17 interaction. Evaluation of the p17 antagonist activity of a panel of biotechnological heparins derived by chemical sulfation of the *Escherichia coli* K5 polysaccharide revealed that the highly *N*,*O*-sulfated derivative prevents the binding of p17 to both heparin and CXCR1, thus inhibiting p17-driven chemotactic migration of human monocytes with an efficiency that is higher than those of heparin and HS. Here, we characterized at a molecular level the interaction of p17 with its cellular receptors, laying the basis for the development of heparin-mimicking p17 antagonists.**

The matrix protein p17 plays important roles in HIV-1 life cycle (1) regulating both early and late stages of viral replication such as P55GAG transport to the membrane (2) and envelope glycoproteins incorporation into nascent virions (3). p17 is also released by HIV-infected cells, being detectable in plasma (4), brain (5), and lymph nodes (6) even in patients successfully treated with highly active antiretroviral therapy (6). Extracellular p17 deregulates the functions of many immune cells involved in AIDS pathogenesis (7): it reduces MIP-1$\alpha$ secretion in activated monocytes (8), induces activated T cell proliferation enhancing HIV replication (9), increases IFN-$\gamma$ and TNF-$\alpha$ production decreasing the ability of IL-4 to down-regulate the secretion of such cytokines in activated peripheral blood mononuclear and natural killer cells (7, 10). Three distinct cellular receptors for p17 have been identified: the chemokine receptors CXCR1 and CXCR2, which mediate p17-driven monocyte migration (11) and endothelial cells proangiogenic activation (12), respectively, and heparan sulfate proteoglycans (HSPGs),[2] tentatively associated to p17-driven cytokine up-regulation in CD4+ lymphocytes (13, 14).

HSPGs typically consist of a core protein and of glycosaminoglycan (GAG) chains made up of unbranched anionic polysaccharides resembling heparin and composed of repeating disaccharides units formed by sulfated uronic acid and hexosamine

* This work was supported by the Istituto Superiore di Sanita (AIDS Grants 40H.51 (to M. R.) and 40G.16 (to A. C.)), the Italian Ministry of University and Scientific Research (to M. R. and A. C.), the Bonino-Pulejo Foundation (Messina, Italy; to A. C.), the Accordo Quadro RL-CNR "Nanoscienze per materiali e applicazioni biomediche," the Interomics Flagship Project, and Italian Ministry of University and Scientific Research Fondo per gli Investimenti della Ricerca di Base-Protocollo HIRMA Grant RBAP11YS7K (to L. M.).

[1] To whom correspondence should be addressed: Sect. of Experimental Oncology and Immunology, Dept. of Molecular and Translational Medicine, viale Europa 11, 25123 Brescia, Italy. Tel.: 39-30-3717315; Fax: 39-30-3717747; E-mail: rusnati@med.unibs.it.

[2] The abbreviations used are: HSPG, heparan sulfate proteoglycan; FGF2, fibroblast growth factor 2; HS, heparan sulfate; RU, resonance units; SPR, surface plasmon resonance; GAG, glycosaminoglycan; PDB, Protein Data Bank; fMLP, *N*-formyl-L-methionyl-L-leucyl-L-phenylalanine; K5NS, *N*-sulfated K5.

residues (15). They are expressed at densities ranging between $10^5$ and $10^6$/cell on the surface of almost all eukaryotic cells where they play co-receptor function for a wide array of heparin-binding cytokines. HSPGs, as well as their structural analog heparin, can be also found in a free form in the extracellular environment (16) where they act as antagonists, sequestering heparin-binding cytokines and hampering their cell surface interactions. The wide distribution and strong interactive capacity of HSPGs made them attractive adhesion molecules for viruses during their evolution. In effect, virus attachment to host cell is often mediated by their interaction with cellular HSPGs (17). Conversely, free heparin-like molecules can inhibit viral infection. Accordingly, a long list of heparin-like polyanions have been so far developed as effective antiviral compounds *in vitro* (18). However, the therapeutical exploitation of these compounds as antiviral drugs is limited by the fact that HSPGs act also as receptors for a wide array of cytokines involved in critical biological events such as cell growth and migration and the maintenance of normal tissue structure and function (16). These considerations call for the development of specific heparin-like compounds able to discriminate between viral and eukaryotic proteins. This, in turn, calls for the fine characterization of the interaction of each viral protein with heparin/HSPGs.

In general, the binding of heparin/HSPGs to viral proteins occurs through negatively charged sulfate groups of the GAG and clusters of positively charged amino acids of the protein also termed "basic motifs" (18). Both the sulfation degree and disposition of sulfate groups along the GAG chain are important in determining the interactive capacity (18). In heparin-binding proteins, unique or multiple basic motifs can be found composed of linear stretches of basic amino acids as in HIV-1 Tat or of conformational cluster of scattered basic amino acids that crowd together in the properly folded protein as in fibroblast growth factor 2 (FGF2) (19).

HIV-infected cells secrete three proteins (Tat, gp120, and p17) that, amazingly, share heparin-binding capacity. Tat/heparin interaction occurs with a dissociation constant ($K_d$) equal to 30–60 nM (20, 21) and is mainly mediated by a linear basic motif $^{49}$RKKRRQRRR$^{57}$ located at the C terminus of the protein (22), with a minor contribution of three other basic amino acids (Lys$^{12}$, Lys$^{41}$, and Arg$^{78}$) spatially enclosed in the native protein (23). At least some 2-*O*-, 6-*O*-, and *N*-positions along the GAG chain need to be sulfated to allow Tat binding (24), and a hexasaccharide is the minimal heparin length that retains Tat-binding capacity (25).

gp120 binds heparin with a $K_d$ equal to 200–600 nM (26, 27). Distinct basic domain are present in the protein, among which the C-terminal "variable loop 3" (18, 28) is implicated in gp120 binding to cell surface HSPGs and consequent HIV infection (26). On the heparin chain, *O*-, but not *N*-sulfated groups are necessary for the binding to gp120 (29–31). An octa/decasaccharide is the minimal heparin size that retains gp120-binding capacity (32).

At variance with Tat and gp120, no data are available about the molecular bases of p17/heparin interaction. The structure of monomeric (33) and trimeric (34) p17 were determined, demonstrating highly similar three-dimensional structures (35). p17 folds into a compact core domain consisting of five $\alpha$-helices and three stranded $\beta$-sheets. $\alpha$-Helices 1–4 form a compact globular domain, whereas the C-terminal helix 5 is partially unfolded, projecting away from the protein, readily accessible for interactions such as that between p17 to P55GAG capsid domains. p17 possesses two basic motifs that may mediate its binding to heparin: in the monomer as well as in the trimer, they are both exposed on the protein surface, one in the N-terminal globular domain of the protein spanning residues 25–34, the other in its partially unfolded C-terminal tail spanning residues 109–115 (see Fig. 1, *A* and *B*). Both of the motifs are not involved in mediating oligomerization of p17, remaining exposed onto the protein surface also when it takes its trimeric form (see also Fig. 1*B*) (34, 35). Here, by integrating computational modeling, site directed mutagenesis of p17, chemical desulfation of heparin, and real time biomolecular interaction analysis by surface plasmon resonance (SPR), we characterized the interaction of p17 to heparin at a molecular level.

## MATERIALS AND METHODS

*Molecular Modeling*—The structures of monomeric p17 were obtained from the Protein Data Bank (PDB) code 1TAM. The structural models of the heparin di-, tetra-, and hexasaccharides were built using the PyMOL program based on their NMR solution structure (PDB code 1HPN). The results for the $^1$C4 conformers were here reported, but similar results were obtained with the $^2$SO conformers (data not shown). Docking of oligosaccharides to p17 was performed with Autodock (version 4.0) (36, 37), which allows flexibility in the heparin structure but uses a rigid body protein approximation to speed up the calculation. Two-step docking simulation was employed. First, a blind docking protocol was used on the monomeric form to predict the bound conformation with no *a priori* knowledge of binding site locations on the molecules (38, 39). To this aim, a grid box encompassing the entire p17 structure was generated to take all possible heparin binding sites into account. In a second set of experiments, a smaller grid, focused on the binding region identified in the blind docking was used to predict the binding mode of the heparin oligosaccharides and to optimize the ligand-protein interactions in the potential heparin binding site. In particular, affinity maps for all the atom types present, as well as an electrostatic map, were computed with a grid spacing of 0.375 Å. The search was carried out with the Lamarckian Genetic Algorithm, the number of generations, energy evaluations, and docking runs were set to 500,000, 2,500,000, and 100, respectively. Eventually, the evaluation with the lowest binding energy was used to analyze ligand pose and the interaction models of heparin oligosaccharides with the monomeric form of p17.

We also performed docking simulations of heparin with the trimeric p17 complex. Relevant to this, the only available three-dimensional structure of trimeric p17 was generated on a protein containing the N-terminal basic motif GKKQYKLKHI (Swiss Prot code P12497, PDB code 1HIW) (34), thus different from the p17 here used for experiments *in vitro* and for molecular modeling with the monomer containing the N-terminal basic motif GKKYKLKHI (Swiss Prot code P04585, PDB code

**TABLE 1**
**Structural features of the GAGs utilized in the present study**

| | MW[a] | $SO_3^-/COO^-$ | Glc-$NSO_3^-$ | Glc-$6SO_3^-$ | IdoA-$2SO_3^-$ | GlcA-$OSO_3^-$[b] | GlcA2,$3SO_3^-$ | Unsulfated GlcA |
|---|---|---|---|---|---|---|---|---|
| | | | % | % | % | % | % | |
| **Heparin/HS** | | | | | | | | |
| Unmodified | 13,600 | 2.14 | 78 | 77 | 59 | | | |
| 2-*O*-Desulfated | 9,600 | 1.60 | 78 | 80 | <5 | | | |
| 6-*O*-Desulfated | 10,300 | 1.50 | 100 | 0 | 50 | | | |
| *N*-Desulfated/*N*-acetylated | 12,300 | 1.50 | 10 | 80 | 60 | | | |
| Heparan sulfate | 18,000 | 1.17 | 42 | 44 | 31 | | | |
| **K5 polysaccharides** | | | | | | | | |
| Unsulfated | 30,000 | 0.00 | 0 | 0 | | 0 | 0 | 100 |
| K5NS | 15,000 | 1.00 | 100 | 0 | | 0 | 0 | 100 |
| K5OSL | 14,000 | 1.41 | 0 | 90 | | <10 | 0 | >90 |
| K5OSH | 11,000 | 3.77 | 0 | 100 | | 0 | 100 | 0 |
| K5NOSL | 13,000 | 1.70 | 100 | 90 | | <10 | 0 | >90 |
| K5NOSH | 15,000 | 3.84 | 100 | 100 | | 30 | 70 | 0 |

[a] MW, molecular weight.
[b] GlcA2$SO_3^-$ or GlcA3$SO_3^-$.

1TAM). Thus, a homology modeling approach was used to generate the three-dimensional structure of the trimeric form of the p17 studied experimentally. Briefly, the PDB code 1HIW was used as a template; sequence alignment of template and target (~93%) was given as input to Modeler program (40) to build three-dimensional structures (Fig. 1*F*). The three-dimensional model was subjected to energy minimization using the Gromacs program (41) and evaluated using PROCHECK (42). The model obtained was submitted to docking simulations and grids focused on three N-terminal binding sites were used to predict the binding mode of heparin oligosaccharide in the relative positions.

All calculations were performed on a Linux Cluster of 32 nodes, each SuperMicro equipped with two processors: the 2.50 GHz INTEL(R) Quad-core and the 16 GB Xeon(R), for 256 total processors and 512 GB of RAM. Figures were realized with the PyMOL Molecular Graphics System (DeLano Scientific, San Carlos, CA).

*Recombinant Proteins*—The coding sequence of HIV-1 matrix protein p17 clade B isolate BH10 (amino acids 1–132) was amplified by PCR with specific primers, allowing the cloning of the p17 sequence into the BamH1 site of the expression vector pGEX-2T (GE Healthcare). p17 N-terminal Lys→Ala mutant, obtained by the substitution of lysines of the N-terminal basic motif with alanine, and the p17 C-terminal K→A mutant, obtained by the same mutations in the C-terminal basic motif, were cloned into the BamH1 site of the pGEX-2T vector using QuikChange site-directed mutagenesis kit (Stratagene, La Jolla, CA). p17Δ36, obtained by the deletion of the C-terminal sequence 97–132, was prepared as described (43). See Fig. 3*A* for a schematic representation of the p17 mutants. p17 proteins and the GST motif alone were purified as described (43). Human recombinant FGF2 was expressed in *Escherichia coli* and purified as described (44). Synthetic 86-amino acid HIV-1 Tat was from Xeptagen (Venezia, Italy). The absence of endotoxin contamination (<0.25 endotoxin units/ml) in protein preparations was assessed by Limulus amoebocyte assay (Associates of Cape Cod, Inc., East Falmouth, MA). Heat denaturation of proteins was obtained by incubation at 95 °C for 5 min.

*Glycosaminoglycans*—Type I HS was from Opocrin (Corlo, Italy). Conventional heparin (13.6 kDa) was obtained from a commercial batch preparation of unfractionated sodium heparin from beef mucosa (Laboratori Derivati Organici S.p.A., Milan, Italy) purified from contaminants (up to 95%) according to described methodologies. Selectively desulfated heparins were a gift of Dr. B. Casu (Ronzoni Institute) (45). Size-defined heparin-derived oligosaccharides were from Iduron (Manchester, UK). The capsular *E. coli* K5 polysaccharide has the same structure as the heparin precursor *N*-acetyl heparosan (46). K5 derivatives were obtained by *N*-deacetylation/*N*-sulfation and/or *O*-sulfation of a single batch of K5 polysaccharide as described (47). For further details on the GAGs used in this study, see Table 1.

*SPR Binding Assay*—SPR measurements were performed on a BIAcore X instrument (GE Healthcare). For the study of p17/heparin interaction, biotinylated heparin was immobilized onto a SA sensorchip containing preimmobilized streptavidin, allowing the immobilization of 159 resonance units (RU), equal to 11.7 fmol/$mm^2$ of heparin. A sensorchip precoated with streptavidin alone was used to evaluate nonspecific binding and for blank subtraction (21). Increasing concentrations of p17 or of its mutants in 10 mM HEPES, pH 7.4 containing 150 mM NaCl, 3 mM EDTA, and 0.005% surfactant P20 (HBS-EP) were injected over the heparin or streptavidin surfaces for 4 min and then washed until dissociation. After each run, the sensorchip was regenerated by injection of 2.0 M NaCl in HBS-EP.

For the study of p17/CXCR1 interaction, anti-GST antibodies were immobilized onto a CM5 sensorchip using standard amine-coupling chemistry. Then, recombinant human CXCR1 with a C-terminal GST tag (10 μg/ml in 50 mM HEPES, pH 7.0, containing 0.01% cholesteryl hemisuccinate Tris salt, 0.1% CHAPS, and 0.33 mM synthetic phospholipid blend (dioleoyl) DOPC:DOPS (7:3 (w/w), Avanti polar lipids) was injected over the anti-GST surface, allowing the immobilization of 1,600 RU, equal to 25 fmol/$mm^2$ of the receptor. A sensor chip coated with anti-GST antibodies was used as a negative control and for blank subtraction (11). Increasing concentrations of p17 or of its mutants in HBS-EP were injected over the CXCR1-coated surfaces for 15 s and then washed until dissociation.

For competition experiments, p17 (500 nM) and increasing concentrations of the different GAGs were preincubated for 10 min at 25 °C and then injected over the heparin or CXCR1 surfaces. Alternatively, p17 was injected over the sensor chips

and allowed to reach an equilibrium binding. Then, increasing concentrations of the various GAGs were injected, and p17 detachment from the surfaces was evaluated. Similar results were obtained in the two experimental approaches (data not shown).

Kinetic parameters were calculated from the sensorgram overlays by using the nonlinear fitting single site model software package BIAevaluation (version 3.2). Only sensorgrams whose fitting gave $\chi 2$ values close to 10 were used (48). Also, $K_d$ was calculated by being fitted with the proper form of Scatchard's equation for the plot of the bound RU at equilibrium *versus* the ligand concentration in solution. All fittings were performed by the software Solar, a least-square minimization procedure based on the Levemburg-Marquardt algorithm.

*Isolation of Human Monocytes and Chemotaxis Assay*—Blood was collected from healthy donors who gave informed consent according to the Helsinki Declaration. All procedures were done under sterile conditions using reagents prepared in endotoxin-free water for clinical use. Human monocytes were isolated from whole blood by Ficoll + Percoll gradient sedimentation (49) and resuspended in migration buffer (phosphate-buffered saline, pH 7.2, containing 1 mM $CaCl_2$, 1 mM $MgCl_2$, and 10% fetal calf serum). Monocyte migration was assessed in 3-$\mu$m pore-size Transwells (BD Biosciences). Aliquots (100 $\mu$l) of cells ($2 \times 10^6$/ml) in migration buffer were added to the top well in the absence or in the presence of heparin, HS, or K5NOSH (at 1 and 10 $\mu$g/ml). Aliquots (600 $\mu$l) of medium with or without p17 (59 nM) or *N*-formyl-L-methionyl-L-leucyl-L-phenylalanine (fMLP, 10 nM) were added to the bottom well. Chemotaxis was performed for 90 min at 37 °C. Then, the filters were removed. After fixation with 1.5% paraformaldehyde, migrated cells were counted in five high-power fields by light microscopy at 10× magnification.

## RESULTS

*Molecular Docking Studies*—To identify the heparin-binding site in the monomeric p17, we performed blind docking simulations in order to predict the binding mode and obtain an estimate of the total interaction energy of the complexes. For all three heparin oligosaccharides used (di-, tetra-, and hexasaccharide), the lowest energy docking was predicted to be located in the N-terminal basic motif of p17 instead of the C-terminal one, although both these motifs are exposed onto the protein surface both in its monomeric and trimeric form. Comparable results were obtained by using either the $^1$C4 or $^2$SO conformers of the three heparin oligosaccharides (data not shown). Thus, local docking simulations were carried out to predict the binding mode of the heparin oligosaccharide and to optimize the ligand-protein interactions in the potential heparin binding site identified. As shown in Fig. 1, *C–F*, and Table 2, p17 is predicted to interact with heparin by an extensive hydrogen-bonding network occurring mainly between the lysines of the N-terminal basic motif of p17 and the negatively charged sulfate groups of heparin. In particular, the heparin disaccharide may form five hydrogen bonds with residues Lys-27, Lys-28, and Lys-30 of p17; the heparin tetrasaccharide may form 10 hydrogen bonds with residues Lys-27, Lys-28, Lys-30, and Lys-32 localized at the beginning of the second $\alpha$-helix; the heparin hexasaccharide may instead bind p17 with 12 hydrogen bonds involving the same residues of the tetrasaccharide plus residue Arg-39 located in the middle of the $\alpha$-helix. Thus, heparin di- and tetrasaccharide may bind to basic amino acids that are contiguous in the basic motif of p17, whereas the heparin hexasaccharide is predicted to bind another residue (Arg-39) that in the folded structure is close to the linear basic motif but in the sequence is distant.

We also evaluated the binding mode of heparin oilgosaccharides with p17 in its trimeric form. As already described under "Materials and Methods," the three-dimensional structure of the trimeric form of the p17 used experimentally (containing the N-terminal basic motif GKKYKLKHI) has not been resolved, prompting to achieve a three-dimensional homology model of its trimeric form by using as a template the available x-ray structure of a p17 trimer containing a N-terminal basic motif GKKQYKLKHI (Swiss Prot code P12497, PDB code 1HIW). As inferred by previous papers (34, 35), the putative heparin-binding N-terminal basic motif GKKYKLKHI remains exposed onto the p17 surface also in the trimeric form (Fig. 1*B*). Molecular docking of the hexasaccharide against modeled complex of p17 was performed on three N-terminal sites. The conformations and interactions of docked hexasaccharides in the binding sites of p17 are shown in Fig. 1*F*. Also, in the trimeric complex of p17, the residues involved in the hydrogen bonds network are the basic residues of the N-terminal motif, Arg-39, and sulfate groups of heparin. The structural analysis of the trimeric form complexed with the ligands suggests a hexasaccharide binding pocket of ~26.5 Å long. The distance between the heparin binding pockets of chain A and B, between chain B and C, and between chain C and A are 26, 23.1, and 17.5 Å, respectively (Fig. 1*F*). These structural considerations suggest that, to interact with more than one binding site, the heparin chain should be composed of at least 18 saccharide units.

*Biochemical Characterization of p17/Heparin Interaction*—SPR was exploited to evaluate the capacity of p17 to bind sensorchip-immobilized heparin, a model that mimics the binding of proteins to cell surface-associated HSPGs (20). p17 interacts with immobilized heparin but not with streptavidin (Fig. 2*A*). When increasing concentrations of p17 were injected onto the heparin surface, the sensorgram overlay shown in Fig. 2*B* was obtained that allowed the calculation of association ($k_{on}$) and dissociation ($k_{off}$) rates and of $K_d$ (as $k_{off}/k_{on}$ ratio, Table 3). Also, equilibrium binding data were used to generate the saturation curve and Scatchard plot regression shown in Fig. 2*C* and used to calculate a $K_d$ value independent from kinetic parameters (Table 3). In conclusion, p17 binds immobilized heparin with a $K_d$ (136–190 nM) that is similar to those of other heparin-binding proteins (Table 3).

To evaluate whether a proper three-dimensional configuration was necessary to p17 to bind heparin, the protein was incubated for 5 min at 95 °C and immediately analyzed in SPR for its capacity to bind to immobilized heparin. FGF2 and Tat were used as controls because their interactions with heparin were already demonstrated to depend on conformational and linear basic domain and motif, respectively (50, 51). As expected, incubation at 95 °C for 5 min causes the complete loss of FGF2

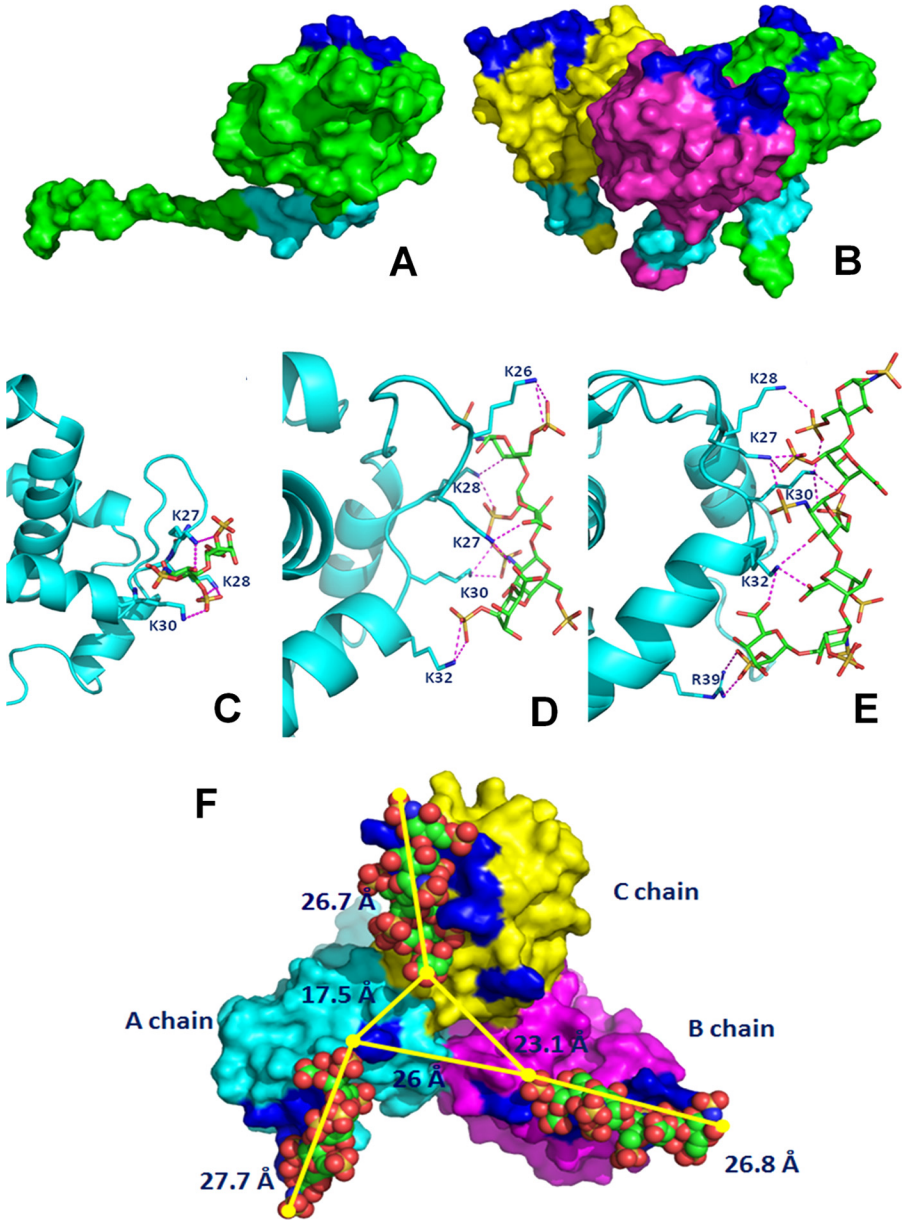


FIGURE 1. Shown is the localization of basic motifs in monomeric (*A*) and trimeric (*B*) p17. The proteins are shown as Connolly surface. The chains are colored in *green*, *yellow*, and *magenta*. The N-terminal and C-terminal basic motifs are labeled in *blue* and *cyan*, respectively. Predicted binding modes between the N-terminal basic motif of p17 and heparin di- (*C*), tetra- (*D*), and hexasaccharide (*E*) are shown. Shown are stick oligosaccharides (*green*) and the side chains of p17 that interact with them (*cyan*). Protein is shown as a *ribbon*, and the hydrogen bonds are represented by *magenta dotted lines*. *F*, prediction of the binding mode of the heparin hexasaccharide at the three N-terminal sites. The modeled trimeric form of p17 is shown as Connolly surface, A chain, B chain, and C chain are colored in *cyan*, *magenta*, and *yellow*, respectively. The N-terminal basic motifs of each chain are colored in *blue*. The ligands are shown in the Corey, Pauling, and Koltun space filling-model.

**TABLE 2**
**Docking results obtained with Autodock for heparin oligosaccharides binding to the N-terminal basic motif of monomeric p17**

| Oligosaccharide probe molecules | Groups of heparin involved in hydrogen bond | | | | | Total interaction energy of the complex |
|---|---|---|---|---|---|---|
| | 2-*O*-Sulfate | *N*-Sulfate | 6-*O*-Sulfate | Carboxyl | 3-*O*-Sulfate | |
| | | | | | | *kcal/mol* |
| Disaccharide $^{1}$C4 | $Lys^{27}$ | | $Lys^{28}$, $Lys^{30}$ | | $Lys^{27}$ | −13.57 |
| No. of hydrogen bonds | 1 | | 3 | | 1 | |
| Tetrasaccharide $^{1}$C4 | $Lys^{28}$, $Lys^{32}$ | $Lys^{30}$ | $Lys^{26}$ | $Lys^{27}$ | $Lys^{28}$ | −19.06 |
| No. of hydrogen bonds | 3 | 2 | 2 | 2 | 1 | |
| Hexasaccharide $^{1}$C4 | $Lys^{27}$, $Arg^{39}$ | $Lys^{27}$ | $Lys^{28}$, $Lys^{30}$ | $Lys^{32}$ | $Lys^{32}$ | −22.28 |
| No. of hydrogen bonds | 4 | 1 | 4 | 2 | 1 | |

heparin-binding capacity (Table 3). At variance, it does not hamper the heparin-binding capacity of both Tat and p17, inducing only a decrease of the affinity of these interactions (Table 3). Important to note, p17 loses its capacity to bind to CXCR1 when used immediately after its heating (Table 3), indicating its effective unfolding. In conclusion, p17 interaction

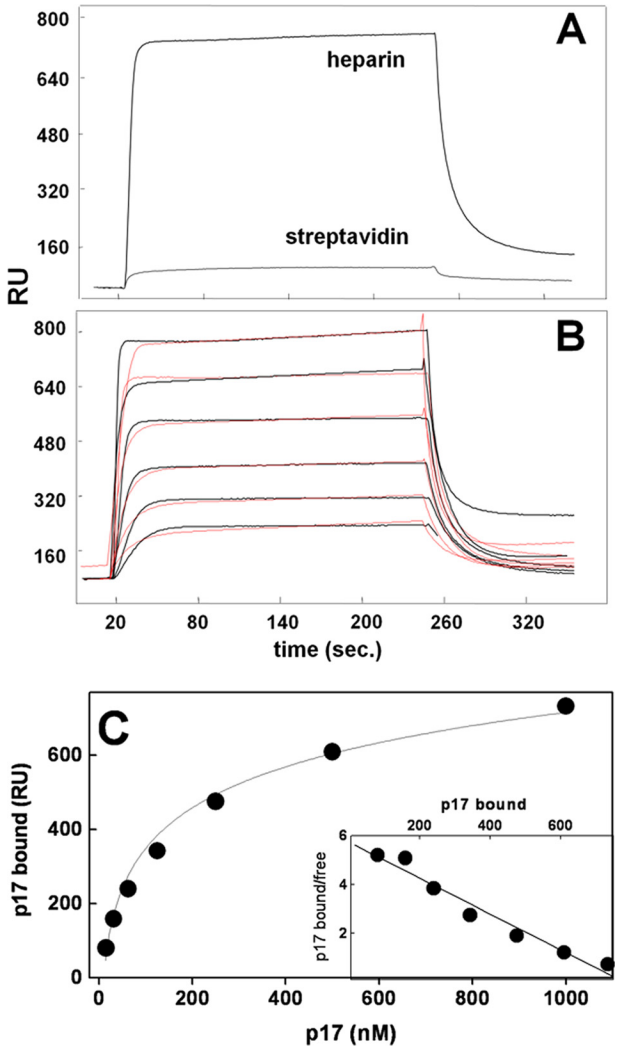


FIGURE 2. **SPR analysis of p17-heparin interaction.** *A*, sensorgrams showing the binding of native p17 (500 nM) to a heparin- or streptavidin-coated sensorchip. *B*, blank-subtracted sensorgrams overlay showing the binding of increasing concentrations of native p17 (1000, 500, 250, 125, 62.5, and 31.25 nM) to a heparin-coated sensorchip. *Black lines* represent the experimental data. *Red lines* represent the fits. In *A* and *B*, the response (in RU) was recorded as a function of time. *C*, saturation curve obtained using the values of RU bound at equilibrium from injection of increasing concentrations of p17 onto a heparin-coated sensorchip. *C*, *inset*: Scatchard plot analysis of the equilibrium binding data shown in *C*. The correlation coefficient of the linear regression was equal to −0.96.

with heparin depends mainly on linear basic motifs rather than on conformational motifs.

Although p17 possess two distinct stretches of basic amino acids ($^{25}$GKKKYKLKHI$^{34}$ and $^{109}$NKSKKKA$^{115}$) that may act as heparin-binding motifs, the blind docking simulations indicated that only the N-terminal one mediates p17 binding to heparin (see above). Thus, two p17 mutants were produced in which the lysines within the N- or C-terminal basic motifs were neutralized by substitution with alanine (p17 N-terminal Lys→Ala and p17 C-terminal Lys→Ala, respectively). Also, taking advantage of the unfolded nature of the C terminus of p17, we produced a deletion mutant (p17Δ36) lacking the last 36-amino acid portion containing the C-terminal basic motif (Fig. 3*A*). As shown in Fig. 3*B*, p17 N-terminal Lys→Ala completely loses its capacity to bind immobilized heparin, whereas p17 C-terminal Lys→Ala retains its heparin-binding capacity (Fig. 3*C* and Table 3). This latter result was paralleled by the observation that also the deletion mutant p17Δ36 retains its capacity to bind heparin (Fig. 3*D* and Table 3). In conclusion, the N-terminal but not the C-terminal basic motif of p17 mediates the interaction of the protein to heparin/HSPGs.

The capacity of heparin to bind to different proteins depends on its degree of sulfation, disposition of the sulfate groups and length of the saccharidic chain (18, 52). To identify the biochemical features of heparin involved in its binding to p17, we exploited a SPR competition assay already used to evaluate the HSPGs antagonist capacity of various polyanionic compounds (20). As shown in Fig. 4*A*, both heparin and HS displace p17 from its binding to sensorchip-immobilized heparin in a dose-dependent manner, with the former exerting a stronger inhibition in respect to the latter ($ID_{50}$ = 18 and 80 nM, respectively). As HS is less sulfated than heparin ($SO_3^-/COO^-$ ratio = 0.93 and 2.14, respectively, see Table 1), it can be concluded that the degree of sulfation is important in determining the p17-binding capacity of heparin/HS.

Next, a series of selectively desulfated heparin (Table 1) was evaluated for their capacity to bind p17. Selective desulfation of 2-*O*, 6-*O*, and *N* positions abolishes the capacity of heparin to interact with p17 (Fig. 4*A*), indicating that all of the sulfate groups of heparin are important for its p17-binding capacity.

Finally, a series of size-defined heparin oligosaccharides were evaluated for their capacity to compete with sensorchip-immobilized full-length heparin for the binding to p17. As shown in Fig. 4*C*, at the doses tested, all of the oligosaccharides except the disaccharide compete with immobilized heparin for the binding to p17 with potencies that increase logarithmically with their size. Taken together, these results indicate that the p17-binding capacity of heparin is greatly influenced by the length of its saccharidic chain.

*Biochemical Characterization of p17-CXCR1 Interaction*—In addition to HSPGs, also CXCR1 acts as p17 receptor on leukocytes (11). Interestingly, the extracellular N-terminal domain of CXCR1 is highly negatively charged (53), and the N-terminal basic motif $^{25}$GKKKYKLKHI$^{34}$ of p17 partially overlaps with the p17 receptor binding domain $^{9}$SGGELDRWEKIRLRPGGKKK$^{28}$ (54). These observations prompted us to investigate whether neutralization of the basic amino acids of the N-terminal basic motif of p17 affected the interaction of the protein to the chemokine receptor. The interaction of wild type p17 with CXCR1 has been already characterized (11). Here, we observed that p17 N-terminal Lys→Ala, but not p17 C-terminal Lys→Ala, completely loses its capacity to bind to CXCR1 (Fig. 5 and Table 3), indicating that, in addition to heparin/HSPGs, the N-terminal basic motif of p17 is also required for its binding to CXCR1.

*Biotechnological Heparins as p17 Antagonists*—K5 derivatives produced by chemical sulfation of *N*- or *O*-positions are endowed with defined sulfation patterns and with the capacity to hamper different biological activities of both Tat and gp120 (31, 55). Here, we assessed the p17-binding and antagonist capacity of a panel of K5 derivatives including the following: *N*-sulfated K5 (K5NS), *O*-sulfated K5 with low and high degrees of sulfation (K5OSL and K5OSH) and *N*,*O*-sulfated K5 with low

**TABLE 3**

**Binding parameters of the interaction of p17 and p17 mutants to heparin and CXCR1**

$k_{on}$ and $k_{off}$ are reported. $K_d$ value was either derived from the $k_{off}/k_{on}$ ratio and by Scatchard plot analysis of the equilibrium binding data. The results shown are representative of other two that gave similar results. For a comparison, the binding parameters of native or heat-denatured FGF2 and Tat are reported. *n.d.*, not determinable; *n.c.*, not calculated.

| | $k_{on}$ | $k_{off}$ | $K_d(k_{on}/k_{off})$ | $K_d$ at equilibrium |
|---|---|---|---|---|
| | *1/M*s | *1/s* | *M* | *M* |
| **Control proteins-heparin** | | | | |
| Native FGF2 | $8.14 \times 10^3$ | $3.20 \times 10^{-4}$ | $3.9 \times 10^{-8}$ | n.c. |
| Heat-denatured FGF2 | n.d. | n.d. | n.d. | n.d. |
| Native Tat | $4.58 \times 10^4$ | $2.07 \times 10^{-3}$ | $4.5 \times 10^{-8}$ | n.c. |
| Heat-denatured Tat | $5.89 \times 10^3$ | $1.37 \times 10^{-3}$ | $2.3 \times 10^{-7}$ | n.c. |
| **p17-heparin** | | | | |
| Native p17 | $3.39 \times 10^5$ | 0.0643 | $1.9 \times 10^{-7}$ | $1.36 \times 10^{-7}$ |
| Heat-denatured p17 | $4.32 \times 10^5$ | 0.217 | $5.03 \times 10^{-7}$ | $4.23 \times 10^{-7}$ |
| p17 N-terminal Lys→Ala | n.d. | n.d. | n.d. | n.d. |
| p17 C-terminal Lys→Ala | $8.14 \times 10^5$ | 0.247 | $3.05 \times 10^{-7}$ | $1.02 \times 10^{-6}$ |
| p17Δ36 | $1.70 \times 10^4$ | $1.72 \times 10^{-3}$ | $1.01 \times 10^{-7}$ | $3.13 \times 10^{-7}$ |
| **p17-CXCR1** | | | | |
| Native p17 | $5.89 \times 10^4$ | 0.102 | $1.73 \times 10^{-6}$ | n.c. |
| Heat-denatured p17 | n.d. | n.d. | n.d. | n.d. |
| p17 N-terminal Lys→Ala | n.d. | n.d. | n.d. | n.d. |
| p17 C-terminal Lys→Ala | $3.22 \times 10^5$ | 0.128 | $3.97 \times 10^{-7}$ | n.c. |

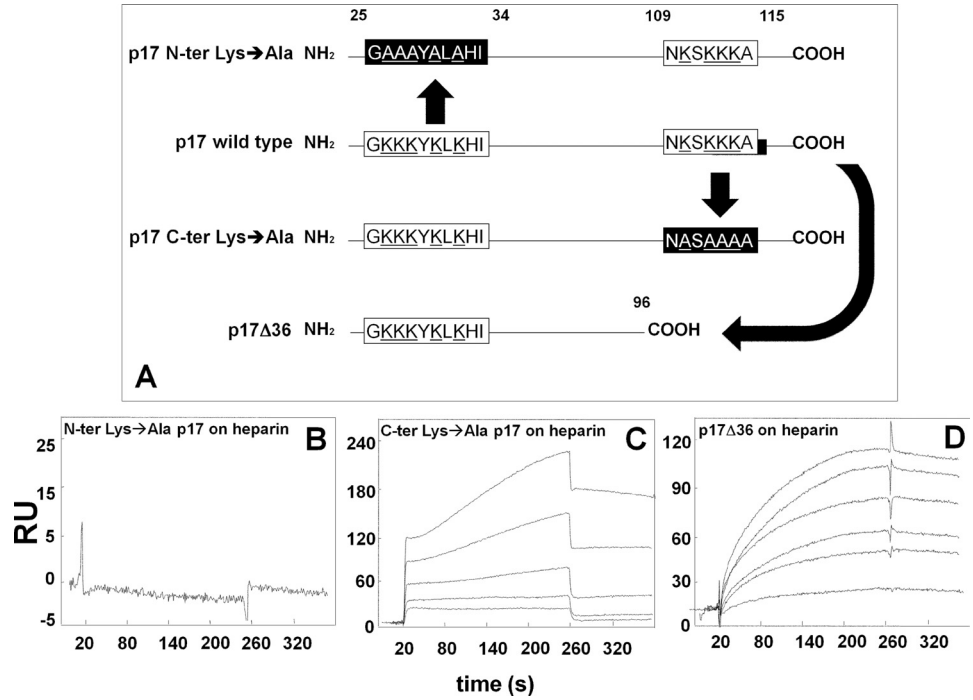


FIGURE 3. **SPR analysis of the interaction of p17 mutants with heparin.** *A*, schematic representation of the p17 mutants used in the present work. The N- and C-terminal basic motifs of p17 (*white boxes*) were deleted or neutralized (*black boxes*) by substituting positively charged lysine with alanine (*underlined*). Blank-subtracted sensorgrams showing the binding of p17 N-terminal (*N-ter*) Lys→Ala (500 nM) (*B*), p17 C-terminal (*C-ter*) Lys→Ala (500, 250, 125, 62.5, and 31.25 nM) (*C*) and p17Δ36 (950, 900, 800, 500, 250, and 100 nM) (*D*) to a heparin-coated sensorchip. The response (in RU) was recorded as a function of time.

and high degrees of sulfation (K5NOSL and K5NOSH) (Tab. 1). As shown in Fig. 6*A*, K5NOSH inhibits the binding of p17 to immobilized heparin with a potency that is higher than that of unmodified heparin ($ID_{50}$ = 2.5 and 18 nM, respectively). K5NS, K5OSL, K5NOSL and K5OSH are less effective ($ID_{50}$ = 30.0, 60.0, 56.0 and 70.0 nM respectively). If compared with the other sulfated derivatives, unsulfated K5 exerts a very limited inhibition (less than 40%) when assayed at 100 nM, suggesting that the contribution of the backbone sugar in p17 interaction is limited in respect to the contribution of sulfate groups. Except for K5NS and K5OSH (discussed below), a clear correlation exists between the $SO_3^-/COO^-$ ratio and the p17-heparin inhibitory capacity of the GAGs tested (Fig. 6*A*, *inset*), further sustaining the importance of the sulfation degree in the p17-binding capacity of heparin/HSPGs.

We then evaluated the ability of the K5 derivatives to inhibit the interaction of p17 to surface-immobilized CXCR1. Preliminary assays demonstrated that the GAGs tested do not bind directly to sensorchip-immobilized CXCR1 (data not shown). As shown in Fig. 6*B*, K5NOSH inhibits p17-CXCR1 interaction with the highest efficiency ($ID_{50}$ = 2.6 nM) followed by K5NS, K5OSL, K5NOSL, and K5OSH ($ID_{50}$ = 48.0, 57.0, and 90.0 nM, respectively). Instead, K5OSL, and unsulfated K5 were ineffective. Heparin and HS are weak inhibitors of the p17-CXCR1 interaction ($ID_{50}$ = 70.0 and 250.0 nM, respectively). There is no statistical correlation between the $SO_3^-/COO^-$ ratio and the

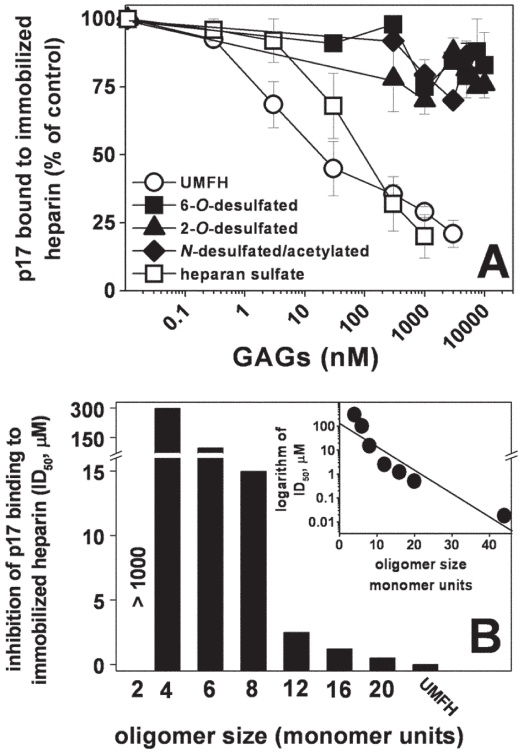


FIGURE 4. **Effect of chemically modified heparins or size-defined oligosaccharides on the interaction of p17 to immobilized heparin.** Selectively desulfated heparins (*A*) or size-defined heparin oligosaccharides (*B*) were evaluated for their capacity to inhibit the interaction of p17 with sensorchip-immobilized heparin. In *A*, the responses were plotted as percentage of the binding of p17 measured in the absence of free GAGs. Each point is the mean ± S.E. of three separate determinations. In *B*, the responses were plotted as $ID_{50}$ of inhibition. The experiment shown is representative of another one that gave similar results. *UMFH*, unmodified heparin. *B*, *inset*, the logarithm of the potency ($ID_{50}$) of the various size-defined heparin oligosaccharides in inhibiting the binding of p17 to immobilized heparin were plotted against their length (monomer units). The correlation coefficient of the linear regression was equal to −0.93.

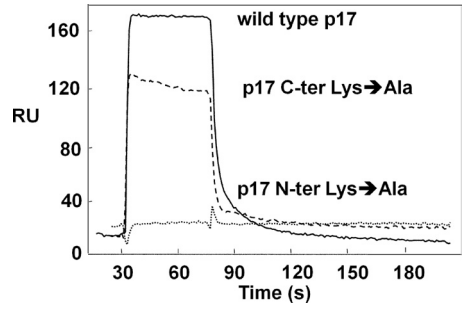


FIGURE 5. **SPR analysis of the interaction of p17 mutants with CXCR1.** Blank-subtracted sensorgrams showing the binding of wild type p17 (*continuous line*), p17 C-terminal (*C-ter*) Lys→Ala (*dashed line*), and p17 N-terminal (*N-ter*) Lys→Ala (*dotted line*) (all at 2 μM) to a CXCR1-coated sensorchip. The response in RU was recorded as a function of time.

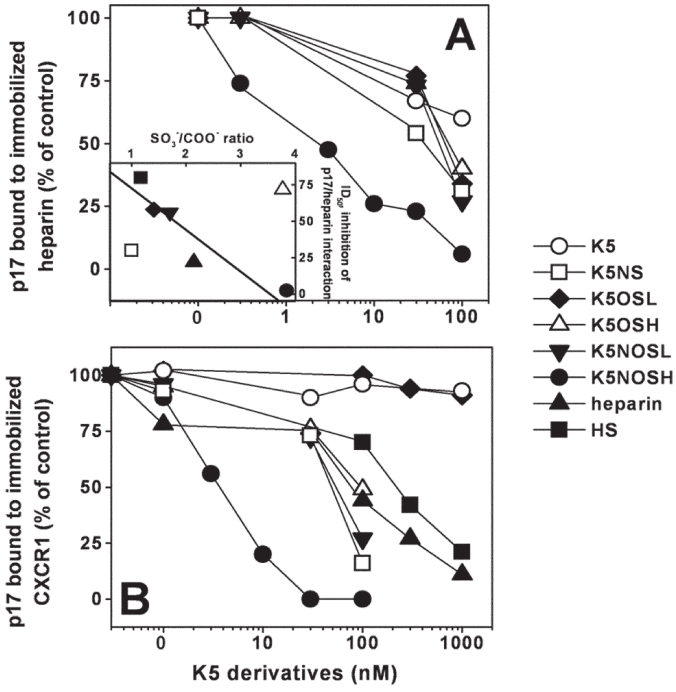


FIGURE 6. **Effect of biotechnological heparins on the interaction of p17 to its receptors.** K5 derivatives were evaluated for their capacity to inhibit the interaction of p17 with heparin (*A*) or CXCR1 (*B*) immobilized to a sensorchip. The responses were plotted as percentage of the binding of p17 measured in the absence of any free GAG. Each point is the mean ± S.E. of three separate determinations. *A*, *inset*, the potency ($ID_{50}$) of the various GAGs in inhibiting the binding of p17 to immobilized heparin were plotted against their $SO_3^-/COO^-$ ratio. The correlation coefficient of the linear regression was equal to −0.96.

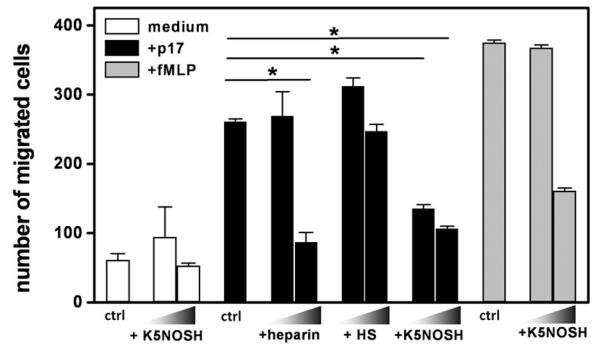


FIGURE 7. **Effect of heparin, HS and K5NOSH on monocyte migration induced by p17.** Monocytes in the absence (control, *ctrl*) or in the presence of heparin, HS and K5NOSH (all at 1 and 10 μg/ml) were added to the top well, whereas medium alone or containing p17 (59 nM) or fMLP (10 nM) was added to the bottom well. *Bars* represent the mean ± S.D. of three independent experiments performed in duplicate. Statistical analysis was performed using GraphPad Prism software (version 5, GraphPad Software, Inc.) and one-way analysis of varaince and Bonferroni's post test was used to compare data. *, $p < 0.01$ statistically different compared with p17-stimulated cells. *NT*, not treated cells.

p17-CXCR1 inhibitory capacity of the various GAGs tested (data not shown).

Both HSPGs and CXCR1 have been implicated in p17-induced activation of leukocytes (11, 14). Because K5NOSH inhibits the interaction of p17 with both heparin and CXCR1, we evaluated its capacity to prevent p17-dependent migration of monocytes. Heparin and HS, which efficiently inhibit p17 binding to heparin but not to CXCR1, were used as controls. As shown in Fig. 7, K5NOSH efficiently inhibits monocyte migration to p17 both at 1 and 10 μg/ml, whereas heparin shows a significant reduced inhibitory potency, as it is active only at 10 μg/ml. HS was ineffective, however, at both the concentrations tested.

To exclude that K5NOSH aspecifically inhibit cell migration, the assay was repeated with fMLP instead of p17. As shown in Fig. 7, K5NOSH does not affect fMLP-driven migration of monocytes when tested at 1 μg/ml, exerting a 50% inhibition only at doses ten times higher. In addition, K5NOSH does not

affect the basal monocytes migration measured in the presence of medium alone.

## DISCUSSION

HIV-infected cells release Tat, gp120, and p17 proteins that, acting in a cytokine-like manner, target uninfected leukocytes (56, 57), neurons (58–60), and endothelial cells (20, 60, 61) inducing various biological effects that, in turn, favor viral spread and the onset of AIDS-associated diseases. Some of these effects depend on the interaction of the viral proteins with HSPGs expressed on the surface of target cells (18, 52, 62), making this class of receptors a promising nodal targets for the development of "multitarget" anti-HIV drugs. This aim requires the fine characterization of the molecular bases of the interaction of the viral proteins with heparin/HSPGs, a study that has been already performed for Tat and gp120, leading to the development of heparin-like compounds endowed with gp120 and/or Tat antagonist capacity (18, 52, 62). Differently, the characterization of the interaction of p17 with heparin/HSPGs has not been performed yet. Here, we report about the biochemical features of p17 and of heparin that govern their interaction.

p17 unfolding does not hamper its binding to heparin, causing only a 3-fold reduction of the affinity of the interaction. Interestingly, a similar behavior has been observed also for Tat, whose interaction with heparin depends mainly on a $^{49}$RKKRRQRRR$^{57}$ linear basic motif with additional but limited contribution given by three other spatially enclosed basic amino acids (Lys$^{12}$, Lys$^{41}$, and Arg$^{78}$) (22, 23). It is thus tentative to hypothesize that also for p17, the main contribution to heparin interaction derives from linear basic motifs, with a minor role played by tridimensional structures. At variance, p17 unfolding hampers its binding to CXCR1 indicating that, for this interaction, the N-terminal basic domain (along with additional structures) need to be presented to the chemokine receptor in a proper tridimensional conformation.

In effect, p17 possess two linear basic motifs: the first in its N-terminal globular part, the second in its partially unfolded C-terminal tail, a region readily accessible to interactions both in the monomeric and trimeric forms of p17. Nevertheless, neutralization or deletion of the C-terminal basic motif does not abolish the heparin-binding capacity of p17, although neutralization of the N-terminal basic motif causes a complete loss of p17 heparin-binding capacity, indicating that this motif is the main responsible for the interaction of p17 with the GAG. Interestingly, independent studies have revealed that the N-terminal but not the C-terminal basic motif of p17 is required to other p17 biological activities, such as HIV particle production and infectivity (3, 63).

As already mentioned, however, heat denaturation induces a 3-fold decrease of the p17 affinity for heparin, suggesting that, in addition to the linear N-terminal basic motif, additional points of interaction with the GAG may originate after p17 folding. In effect, molecular docking studies predicted that the binding of heparin to p17 is characterized by an extensive hydrogen-bonding network of interactions occurring mainly between the negatively charged groups of heparin and the contiguous lysines of the N-terminal basic motif. However, an additional contribution to the interaction seems to be given by an arginine localized at position 39 in the second $\alpha$-helix that is distant in the sequence but close to the stretch of lysines in the folded structure. Thus, heat denaturation could unfold the $\alpha$ helix, distancing Arg$^{39}$ from the N-terminal basic motif, reducing the width of the zone of interaction and thus the affinity of the binding. Further site-directed mutagenesis experiments and SPR analyses are required to formally prove this possibility.

Different biochemical features of heparin impact its capacity to bind p17. (i) Sulfate groups, rather than the carbonic backbone of heparin, mediate its interaction with p17. Indeed, unsulfated K5 polysaccharide shows a very limited p17 binding capacity. Also, among the GAGs tested, a correlation exists between their sulfation degree and their capacity to inhibit p17/heparin interaction. (ii) Other than the sulfation degree, also the specific disposition of the sulfate groups along the heparin chain impacts its p17-binding capacity: in effect, the p17 antagonist capacity of K5NS is higher than that of K5OSL despite its lower $SO_3^-$/COOH (1.0 and 1.41, respectively, Table 1). Also, K5OSH and K5OSL exert a similar p17 antagonist activity despite the fact that the former is endowed with a $SO_3^-$COOH ratio that is three times higher that the latter (3.77 and 1.41, respectively (Table 1 and Fig. 4*B*). Thus, *N*-sulfate groups seem to be particularly important for the interaction of K5 derivatives with p17, whereas an increase in *O*-sulfation does not contribute further to their p17-binding capacity. Accordingly, by plotting the percent of sulfation of the different positions in the GAGs (see Table 1) *versus* their capacity to inhibit the binding of p17 to immobilized heparin, a moderate correlation ($r = -0.70$) can be calculated only for the Glc-$NSO_3^-$ position (data not shown). (iii) Epimerization of the GAGs decreases their p17-binding capacity. Indeed, non-epimerized K5NS is a stronger p17 binder than epimerized 6-*O*- and 2-*O*-desulfated heparins, despite these two latter GAGs retain *N*-sulfation and a higher sulfation degree ($SO_3^-$/COOH = 1.0 for K5NS and to 1.5 for the two desulfated heparins, see Table 1). (iv) The p17-binding capacity of heparin depends on the length of its saccharidic chain. Indeed, size-defined heparin oligosaccharides, all endowed with a similar degree and disposition of sulfate groups, compete with immobilized heparin for the binding to p17 with potencies that increase logarithmically with the length of their saccharidic chain. Actually, in the competition binding assay, the hexa- and tetra-, but not the disaccharide prevents p17 binding to immobilized heparin. However, in a direct binding assay with p17 immobilized to the sensorchip, we were able to demonstrate that also the disaccharide binds the protein (data not shown), indicating that its lack of effect in the competition assay is due to its low inhibitory potency and the dilution of the sample available. In conclusion, the results from the binding assays support the data from computational modeling that predict that also very short heparin sequences can bind to p17.

According to the results of the molecular docking models, a heparin hexasaccharide accommodates a single p17 basic motif (Fig. 1). However, docking simulations of the hexasaccharide against the trimeric p17 predict a length of ~26.5 Å of the N-terminal binding site and a distance between two binding sites of ~23 Å, suggesting that a heparin chain should be com-

posed of at least 18 monosaccharides to interact simultaneously with more than one heparin binding pockets favoring cooperative p17 bindings and its oligomerization, as already demonstrated for HIV-1 Tat and other chemokines (25, 64). In effect, we observed that the p17 antagonist capacity of heparin oligosaccharides increases logarithmically with their length (Fig. 4*B*) and that full-length heparin effectively induces p17 oligomerization.[3] Further computational studies with longer heparin chains should be needed to appropriately characterize the interaction of heparin with the trimeric p17 complex.

p17 binds heparin with an affinity ($K_d$ = 190 nM) that is similar to that of gp120 ($K_d$ = 200–600 nM) and only three times lower than that of Tat ($K_d$ = 30–60 nM), two HIV proteins that exploit HSPGs to mediate important biological effects (see Introduction). On the other hand, p17 binds to HSPGs on leukocytes, and although no formal demonstration has been provided, this interaction has been tentatively associated to the modulation of inflammatory cytokines expression (14). Even if the possibility that p17-HSPGs interaction directly induces some biological activity in the cell cannot be ruled out, it is likely that HSPGs may instead act as typical co-receptors, which, by binding p17, cause its conformational modifications/oligomerization that, in turn, ameliorate its binding to signaling receptors such as CXCR1. Relevant to this point, SPR analysis revealed that p17 binds both CXCR1 and heparin with $K_d$ values that are significantly higher that the concentrations required to induce leukocyte migration (11), suggesting that, *in vivo*, the "productive" interaction of p17 with cells consists of the formation of a p17-HSPG-CXCR1 ternary complex, in which the affinity of the interactions is increased, as already demonstrated for other heparin-binding cytokines (65). This possibility is also sustained by the observation that in the trimeric form of p17 the N-terminal basic motif remains exposed onto the protein surface (34), readily accessible to receptors for multiple interactions. Further experiments are required to clarify the complex relationship existing between p17, HSPGs and chemochine receptors at the surface of target cells.

The involvement of p17 N-terminal basic motif in the binding to both heparin and CXCR1 is not surprising. Indeed, the basic motif of Tat is involved in the binding to HSPGs, integrins and VEGFR2 (61). Interestingly, selected K5 derivatives prevent Tat interaction with all these receptors, inhibiting the consequent biological activities (55). Here, we have shown that K5NOSH prevents the binding of p17 to both HSPGs and CXCR1, inhibiting p17-driven monocyte chemotaxis. Thus, the basic motif of p17 (as well as those of other viral proteins) can be considered as nodal motifs implicated in multiple interactions, thus emerging as preferential aim for the development of multitarget drugs interfering with different receptors (18). Finally, it is also worth noting that K5 derivatives are able to interfere with other HIV proteins (Tat and gp120, see above), suggesting the possibility to use K5 derivatives as template for the development of drugs endowed with an interesting anti-HIV multitarget action, directed against both different receptors of a given HIV protein and against different HIV proteins (18).

[3] A. Bugatti, C. Giagulli, P. D'ursi, A. Caruso, and M. Rusnati, manuscript in preparation.

*Acknowledgments—We thank P. Bergese and L. Ravelli for Solar (the software for Langmuir analysis), M. Moscatelli for the setting up of computational studies, and G. Zoppetti for helpful discussion.*

## REFERENCES


1. Fiorentini, S., Riboldi, E., Facchetti, F., Avolio, M., Fabbri, M., Tosti, G., Becker, P. D., Guzman, C. A., Sozzani, S., and Caruso, A. (2008) HIV-1 matrix protein p17 induces human plasmacytoid dendritic cells to acquire a migratory immature cell phenotype. *Proc. Natl. Acad. Sci. U.S.A.* **105,** 3867–3872
2. Bryant, M., and Ratner, L. (1990) Myristoylation-dependent replication and assembly of human immunodeficiency virus 1. *Proc. Natl. Acad. Sci. U.S.A.* **87,** 523–527
3. Cannon, P. M., Matthews, S., Clark, N., Byles, E. D., Iourin, O., Hockley, D. J., Kingsman, S. M., and Kingsman, A. J. (1997) Structure-function studies of the human immunodeficiency virus type 1 matrix protein, p17. *J. Virol.* **71,** 3474–3483
4. Budka, H. (1990) Human immunodeficiency virus (HIV) envelope and core proteins in CNS tissues of patients with the acquired immune deficiency syndrome (AIDS). *Acta Neuropathol.* **79,** 611–619
5. Popovic, M., Tenner-Racz, K., Pelser, C., Stellbrink, H. J., van Lunzen, J., Lewis, G., Kalyanaraman, V. S., Gallo, R. C., and Racz, P. (2005) Persistence of HIV-1 structural proteins and glycoproteins in lymph nodes of patients under highly active antiretroviral therapy. *Proc. Natl. Acad. Sci. U.S.A.* **102,** 14807–14812
6. Fiorentini, S., Giagulli, C., Caccuri, F., Magiera, A. K., and Caruso, A. (2010) HIV-1 matrix protein p17: a candidate antigen for therapeutic vaccines against AIDS. *Pharmacol. Ther.* **128,** 433–444
7. De Francesco, M. A., Baronio, M., Fiorentini, S., Signorini, C., Bonfanti, C., Poiesi, C., Popovic, M., Grassi, M., Garrafa, E., Bozzo, L., Lewis, G. K., Licenziati, S., Gallo, R. C., and Caruso, A. (2002) HIV-1 matrix protein p17 increases the production of proinflammatory cytokines and counteracts IL-4 activity by binding to a cellular receptor. *Proc. Natl. Acad. Sci. U.S.A.* **99,** 9972–9977
8. De Francesco, M. A., Poiesi, C., Ricotta, D., and Manca, N. (2006) HIV p17 reverses the anti-inflammatory activity of IL-4 on IL-15 stimulated monocytes and modulates their ability to secrete MIP-1 $\alpha$. *Virus Res.* **118,** 170–177
9. De Francesco, M. A., Caruso, A., Fallacara, F., Canaris, A. D., Dima, F., Poiesi, C., Licenziati, S., Corulli, M., Martinelli, F., Fiorentini, S., and Turano, A. (1998) HIV p17 enhances lymphocyte proliferation and HIV-1 replication after binding to a human serum factor. *Aids* **12,** 245–252
10. Vitale, M., Caruso, A., De Francesco, M. A., Rodella, L., Bozzo, L., Garrafa, E., Grassi, M., Gobbi, G., Cacchioli, A., and Fiorentini, S. (2003) HIV-1 matrix protein p17 enhances the proliferative activity of natural killer cells and increases their ability to secrete proinflammatory cytokines. *Br. J. Haematol.* **120,** 337–343
11. Giagulli, C., Magiera, A. K., Bugatti, A., Caccuri, F., Marsico, S., Rusnati, M., Vermi, W., Fiorentini, S., and Caruso, A. (2012) HIV-1 matrix protein p17 binds to the IL-8 receptor CXCR1 and shows IL-8-like chemokine activity on monocytes through Rho/ROCK activation. *Blood* **119,** 2274–2283
12. Caccuri, F., Giagulli, C., Bugatti, A., Benetti, A., Alessandri, G., Ribatti, D., Marsico, S., Apostoli, P., Slevin, M. A., Rusnati, M., Guzman, C. A., Fiorentini, S., and Caruso, A. (2012) HIV-1 matrix protein p17 promotes angiogenesis via chemokine receptors CXCR1 and CXCR2. *Proc. Natl. Acad. Sci. U.S.A.* **109,** 14580–14585
13. Poiesi, C., De Francesco, M. A., Baronio, M., and Manca, N. (2008) HIV-1 p17 binds heparan sulfate proteoglycans to activated CD4(+) T cells. *Virus Res.* **132,** 25–32
14. De Francesco, M. A., Baronio, M., and Poiesi, C. (2011) HIV-1 p17 matrix protein interacts with heparan sulfate side chain of CD44v3, syndecan-2, and syndecan-4 proteoglycans expressed on human activated CD4+ T cells affecting tumor necrosis factor $\alpha$ and interleukin 2 production. *J. Biol. Chem.* **286,** 19541–19548
15. Lindahl, U., Lidholt, K., Spillmann, D., and Kjellén, L. (1994) More to

"heparin" than anticoagulation. *Thromb. Res.* **75,** 1–32
16. Turnbull, J., Powell, A., and Guimond, S. (2001) Heparan sulfate: decoding a dynamic multifunctional cell regulator. *Trends Cell Biol.* **11,** 75–82
17. Spillmann, D. (2001) Heparan sulfate: anchor for viral intruders? *Biochimie* **83,** 811–817
18. Rusnati, M., Vicenzi, E., Donalisio, M., Oreste, P., Landolfo, S., and Lembo, D. (2009) Sulfated K5 *Escherichia coli* polysaccharide derivatives: A novel class of candidate antiviral microbicides. *Pharmacol. Ther.* **123,** 310–322
19. Coltrini, D., Rusnati, M., Zoppetti, G., Oreste, P., Grazioli, G., Naggi, A., and Presta, M. (1994) Different effects of mucosal, bovine lung and chemically modified heparin on selected biological properties of basic fibroblast growth factor. *Biochem. J.* **303,** 583–590
20. Bugatti, A., Urbinati, C., Ravelli, C., De Clercq, E., Liekens, S., and Rusnati, M. (2007) Heparin-mimicking sulfonic acid polymers as multitarget inhibitors of human immunodeficiency virus type 1 Tat and gp120 proteins. *Antimicrob. Agents Chemother.* **51,** 2337–2345
21. Rusnati, M., Urbinati, C., Caputo, A., Possati, L., Lortat-Jacob, H., Giacca, M., Ribatti, D., and Presta, M. (2001) Pentosan polysulfate as an inhibitor of extracellular HIV-1 Tat. *J. Biol. Chem.* **276,** 22420–22425
22. Goldstein, G. (1996) HIV-1 Tat protein as a potential AIDS vaccine. *Nat. Med.* **2,** 960–964
23. Ai, J., Xin, X., Zheng, M., Wang, S., Peng, S., Li, J., Wang, L., Jiang, H., and Geng, M. (2008) A triad of lys12, lys41, arg78 spatial domain, a novel identified heparin binding site on tat protein, facilitates tat-driven cell adhesion. *PLoS One* **3,** e2662
24. Rusnati, M., Coltrini, D., Oreste, P., Zoppetti, G., Albini, A., Noonan, D., d'Adda di Fagagna, F., Giacca, M., and Presta, M. (1997) Interaction of HIV-1 Tat protein with heparin. Role of the backbone structure, sulfation, and size. *J. Biol. Chem.* **272,** 11313–11320
25. Rusnati, M., Tulipano, G., Spillmann, D., Tanghetti, E., Oreste, P., Zoppetti, G., Giacca, M., and Presta, M. (1999) Multiple interactions of HIV-I Tat protein with size-defined heparin oligosaccharides. *J. Biol. Chem.* **274,** 28198–28205
26. Moulard, M., Lortat-Jacob, H., Mondor, I., Roca, G., Wyatt, R., Sodroski, J., Zhao, L., Olson, W., Kwong, P. D., and Sattentau, Q. J. (2000) Selective interactions of polyanions with basic surfaces on human immunodeficiency virus type 1 gp120. *J. Virol.* **74,** 1948–1960
27. Crublet, E., Andrieu, J. P., Vivès, R. R., and Lortat-Jacob, H. (2008) The HIV-1 envelope glycoprotein gp120 features four heparan sulfate binding domains, including the co-receptor binding site. *J. Biol. Chem.* **283,** 15193–15200
28. Ping, L. H., Nelson, J. A., Hoffman, I. F., Schock, J., Lamers, S. L., Goodman, M., Vernazza, P., Kazembe, P., Maida, M., Zimba, D., Goodenow, M. M., Eron, J. J., Jr., Fiscus, S. A., Cohen, M. S., and Swanstrom, R. (1999) Characterization of V3 sequence heterogeneity in subtype C human immunodeficiency virus type 1 isolates from Malawi: underrepresentation of X4 variants. *J. Virol.* **73,** 6271–6281
29. Lopalco, L., Ciccomascolo, F., Lanza, P., Zoppetti, G., Caramazza, I., Leoni, F., Beretta, A., and Siccardi, A. G. (1994) Anti-HIV type 1 properties of chemically modified heparins with diminished anticoagulant activity. *AIDS Res. Hum. Retroviruses* **10,** 787–793
30. Rider, C. C., Coombe, D. R., Harrop, H. A., Hounsell, E. F., Bauer, C., Feeney, J., Mulloy, B., Mahmood, N., Hay, A., and Parish, C. R. (1994) Anti-HIV-1 activity of chemically modified heparins: correlation between binding to the V3 loop of gp120 and inhibition of cellular HIV-1 infection *in vitro*. *Biochemistry* **33,** 6974–6980
31. Vicenzi, E., Gatti, A., Ghezzi, S., Oreste, P., Zoppetti, G., and Poli, G. (2003) Broad spectrum inhibition of HIV-1 infection by sulfated K5 *Escherichia coli* polysaccharide derivatives. *Aids* **17,** 177–181
32. Vivès, R. R., Imberty, A., Sattentau, Q. J., and Lortat-Jacob, H. (2005) Heparan sulfate targets the HIV-1 envelope glycoprotein gp120 coreceptor binding site. *J. Biol. Chem.* **280,** 21353–21357
33. Matthews, S., Barlow, P., Clark, N., Kingsman, S., Kingsman, A., and Campbell, I. (1995) Refined solution structure of p17, the HIV matrix protein. *Biochem. Soc. Trans.* **23,** 725–729
34. Hill, C. P., Worthylake, D., Bancroft, D. P., Christensen, A. M., and Sundquist, W. I. (1996) Crystal structures of the trimeric human immunodeficiency virus type 1 matrix protein: implications for membrane association and assembly. *Proc. Natl. Acad. Sci. U.S.A.* **93,** 3099–3104
35. Massiah, M. A., Worthylake, D., Christensen, A. M., Sundquist, W. I., Hill, C. P., and Summers, M. F. (1996) Comparison of the NMR and X-ray structures of the HIV-1 matrix protein: evidence for conformational changes during viral assembly. *Protein Sci.* **5,** 2391–2398
36. Morris, G. M., Goodsell, D. S., Huey, R., and Olson, A. J. (1996) Distributed automated docking of flexible ligands to proteins: parallel applications of AutoDock 2.4. *J. Comput. Aided Mol. Des.* **10,** 293–304
37. Huey, R., Morris, G. M., Olson, A. J., and Goodsell, D. S. (2007) A semiempirical free energy force field with charge-based desolvation. *J. Comput. Chem.* **28,** 1145–1152
38. Hetényi, C., and van der Spoel, D. (2002) Efficient docking of peptides to proteins without prior knowledge of the binding site. *Protein Sci.* **11,** 1729–1737
39. Hetényi, C., and van der Spoel, D. (2006) Blind docking of drug-sized compounds to proteins with up to a thousand residues. *FEBS Lett.* **580,** 1447–1450
40. Sali, A., and Blundell, T. L. (1993) Comparative protein modelling by satisfaction of spatial restraints. *J. Mol. Biol.* **234,** 779–815
41. Van Der Spoel, D., Lindahl, E., Hess, B., Groenhof, G., Mark, A. E., and Berendsen, H. J. (2005) GROMACS: fast, flexible, and free. *J. Comput. Chem.* **26,** 1701–1718
42. Laskowski, R. A., Rullmannn, J. A., MacArthur, M. W., Kaptein, R., and Thornton, J. M. (1996) AQUA and PROCHECK-NMR: programs for checking the quality of protein structures solved by NMR. *J. Biomol. NMR* **8,** 477–486
43. Giagulli, C., Marsico, S., Magiera, A. K., Bruno, R., Caccuri, F., Barone, I., Fiorentini, S., Andò, S., and Caruso, A. (2011) Opposite effects of HIV-1 p17 variants on PTEN activation and cell growth in B cells. *PLoS One* **6,** e17831
44. Isacchi, A., Statuto, M., Chiesa, R., Bergonzoni, L., Rusnati, M., Sarmientos, P., Ragnotti, G., and Presta, M. (1991) A six-amino acid deletion in basic fibroblast growth factor dissociates its mitogenic activity from its plasminogen activator-inducing capacity. *Proc. Natl. Acad. Sci. U.S.A.* **88,** 2628–2632
45. Inoue, Y., and Nagasawa, K. (1976) Selective *N*-desulfation of heparin with dimethyl sulfoxide containing water or methanol. *Carbohydr. Res.* **46,** 87–95
46. Casu, B., Grazioli, G., Razi, N., Guerrini, M., Naggi, A., Torri, G., Oreste, P., Tursi, F., Zoppetti, G., and Lindahl, U. (1994) Heparin-like compounds prepared by chemical modification of capsular polysaccharide from *E. coli* K5. *Carbohydr. Res.* **263,** 271–284
47. Leali, D., Belleri, M., Urbinati, C., Coltrini, D., Oreste, P., Zoppetti, G., Ribatti, D., Rusnati, M., and Presta, M. (2001) Fibroblast growth factor-2 antagonist activity and angiostatic capacity of sulfated *Escherichia coli* K5 polysaccharide derivatives. *J. Biol. Chem.* **276,** 37900–37908
48. Khalifa, M. B., Choulier, L., Lortat-Jacob, H., Altschuh, D., and Vernet, T. (2001) BIACORE data processing: an evaluation of the global fitting procedure. *Anal. Biochem.* **293,** 194–203
49. Fontana, L., Giagulli, C., Minuz, P., Lechi, A., and Laudanna, C. (2001) 8-Iso-PGF2 $\alpha$ induces $\beta$ 2-integrin-mediated rapid adhesion of human polymorphonuclear neutrophils: a link between oxidative stress and ischemia/reperfusion injury. *Arterioscler. Thromb. Vasc. Biol.* **21,** 55–60
50. Coltrini, D., Rusnati, M., Zoppetti, G., Oreste, P., Isacchi, A., Caccia, P., Bergonzoni, L., and Presta, M. (1993) Biochemical bases of the interaction of human basic fibroblast growth factor with glycosaminoglycans. New insights from trypsin digestion studies. *Eur. J. Biochem.* **214,** 51–58
51. Rusnati, M., Tulipano, G., Urbinati, C., Tanghetti, E., Giuliani, R., Giacca, M., Ciomei, M., Corallini, A., and Presta, M. (1998) The basic domain in HIV-1 Tat protein as a target for polysulfonated heparin-mimicking extracellular Tat antagonists. *J. Biol. Chem.* **273,** 16027–16037
52. Rusnati, M., and Urbinati, C. (2009) Polysulfated/sulfonated compounds for the development of drugs at the crossroad of viral infection and oncogenesis. *Curr. Pharm. Des.* **15,** 2946–2957
53. Fernando, H., Nagle, G. T., and Rajarathnam, K. (2007) Thermodynamic characterization of interleukin-8 monomer binding to CXCR1 receptor N-terminal domain. *FEBS J.* **274,** 241–251
54. Fiorentini, S., Marini, E., Bozzo, L., Trainini, L., Saadoune, L., Avolio, M.,

Pontillo, A., Bonfanti, C., Sarmientos, P., and Caruso, A. (2004) Preclinical studies on immunogenicity of the HIV-1 p17-based synthetic peptide AT20-KLH. *Biopolymers* **76,** 334–343
55. Urbinati, C., Bugatti, A., Oreste, P., Zoppetti, G., Waltenberger, J., Mitola, S., Ribatti, D., Presta, M., and Rusnati, M. (2004) Chemically sulfated *Escherichia coli* K5 polysaccharide derivatives as extracellular HIV-1 Tat protein antagonists. *FEBS Lett.* **568,** 171–177
56. Fiorentini, S., Marini, E., Caracciolo, S., and Caruso, A. (2006) Functions of the HIV-1 matrix protein p17. *New Microbiol.* **29,** 1–10
57. Herbein, G., Gras, G., Khan, K. A., and Abbas, W. (2010) Macrophage signaling in HIV-1 infection. *Retrovirology* **7,** 34
58. Corasaniti, M. T., Maccarrone, M., Nistico, R., Malorni, W., Rotiroti, D., and Bagetta, G. (2001) Exploitation of the HIV-1 coat glycoprotein, gp120, in neurodegenerative studies in vivo. *J. Neurochem.* **79,** 1–8
59. Chauhan, A., Turchan, J., Pocernich, C., Bruce-Keller, A., Roth, S., Butterfield, D. A., Major, E. O., and Nath, A. (2003) Intracellular human immunodeficiency virus Tat expression in astrocytes promotes astrocyte survival but induces potent neurotoxicity at distant sites via axonal transport. *J. Biol. Chem.* **278,** 13512–13519
60. Singh, I. N., Goody, R. J., Dean, C., Ahmad, N. M., Lutz, S. E., Knapp, P. E., Nath, A., and Hauser, K. F. (2004) Apoptotic death of striatal neurons induced by human immunodeficiency virus-1 Tat and gp120: Differential involvement of caspase-3 and endonuclease G. *J. Neurovirol.* **10,** 141–151
61. Rusnati, M., and Presta, M. (2002) HIV-1 Tat protein and endothelium: from protein/cell interaction to AIDS-associated pathologies. *angiogenesis* **5,** 141–151
62. Lembo, D., Donalisio, M., Rusnati, M., Bugatti, A., Cornaglia, M., Cappello, P., Giovarelli, M., Oreste, P., and Landolfo, S. (2008) Sulfated K5 *Escherichia coli* polysaccharide derivatives as wide-range inhibitors of genital types of human papillomavirus. *Antimicrob. Agents Chemother.* **52,** 1374–1381
63. Hearps, A. C., and Jans, D. A. (2007) Regulating the functions of the HIV-1 matrix protein. *AIDS Res. Hum. Retroviruses* **23,** 341–346
64. Hoogewerf, A. J., Kuschert, G. S., Proudfoot, A. E., Borlat, F., Clark-Lewis, I., Power, C. A., and Wells, T. N. (1997) Glycosaminoglycans mediate cell surface oligomerization of chemokines. *Biochemistry* **36,** 13570–13578
65. Rusnati, M., and Presta, M. (1996) Interaction of angiogenic basic fibroblast growth factor with endothelial cell heparan sulfate proteoglycans. Biological implications in neovascularization. *Int. J. Clin. Lab. Res.* **26,** 15–23